Efficient linear and non-linear dynamic analysis and design of RC cooling towers subjected to earthquake

Christian Lang
HOCHTIEF Construction AG, IKS, Frankfurt am Main, Germany

Udo Wittek
Department of Civil Engineering, Institute of Statics, Technical University of Kaiserslautern, Germany

ABSTRACT: In this paper, a very efficient method for computation of structural response of RC shells of revolution such as natural draught cooling towers is presented using a finite ring element concept. The enhancement of a double curved ring element for consideration of realistic non-linear RC constitutive laws in combination with solution algorithms for dynamic problems is summarized. This shell ring element is implemented in the finite element program system ROSHE (Wittek et al. 2002) where a variety of very powerful analysis tools for computation of linear and non-linear structural response of RC shells of revolution subjected to transient dynamic loading are provided. Special applications of these elements are given within this contribution: Here, aspects of structural modeling are discussed using this special ring element method. Further, the dynamic behaviour and its consequences on the structural design of a modern natural draught cooling tower subjected to horizontal seismic ground acceleration are explained. The results obtained from different analysis methods – equivalent static acceleration method, response spectrum method and transient linear and non-linear dynamic analyses – are compared and discussed.

1 INTRODUCTION

Shells of revolution are frequently found in engineering structures as a special representative of general spatial shell structures. The geometry of these shells is described by a mathematical relation between the height Z and the radius $R(Z)$ of the shell. Thus, by rotating this curve around a given axis, the middle surface of the shell of revolution is obtained.

During the last years, huge effort has been spent in the development and enhancement of highly advanced general shell elements for numerical calculation of arbitrary shell structures by the finite element method accounting for large deformations, rotations, finite strain and arbitrary material laws. In this contribution, a different approach will be used: For the numerical calculation of shells of revolution with axissymmetric geometry, ring elements can be deployed advantageously, both for linear and non-linear structural behaviour with consideration of realistic properties of reinforced concrete. The basic idea is to introduce a Fourier series for the unknown displacement field in circumferential direction of the ring element. Research on ring elements dates back to the early work in the 1960s (Popov et al. 1964) where a very simple conical ring element with constant wall thickness for axissymmetric problems was proposed. The idea of ring elements was enhanced through the years by several researchers. First attempts for consideration of non-linearities of steel material in ring elements within a pseudo-load formulation have been undertaken in the beginning of the 1980's (Wunderlich and Rensch 1981).

In this contribution, the non-linear formulation of an existing linear shell ring element with double curved geometry based on the early works by Leimbach (Leimbach 1973) and Eckstein et al. (Eckstein et al. 1980) with consideration of realistic material laws for reinforced concrete is summarized (Lang 2003). Further, enhancements to non-linear dynamics are presented. Different solution strategies – equivalent static loads, response spectrum method, direct integration and modal superposition – for solving the equations of motion are discussed. With this theoretical background, the earthquake behaviour and design of a modern natural draught cooling tower is studied. Here, non-linear effects arising from uplift and cracking of shell and columns are accounted for in the numerical model.

2 CONSTITUTIVE MODELS FOR RC CONCRETE

2.1 *Stress resultants and section integration*

In Figure 1, a cut-out of a shell of revolution with its body forces and stress resultants is depicted. For general non-linear material response, the section is divided up into a number of layers. By numerical section integration through the depth, membrane forces $n^{\alpha\beta}$ and moments $m^{\alpha\beta}$ are computed using Equation

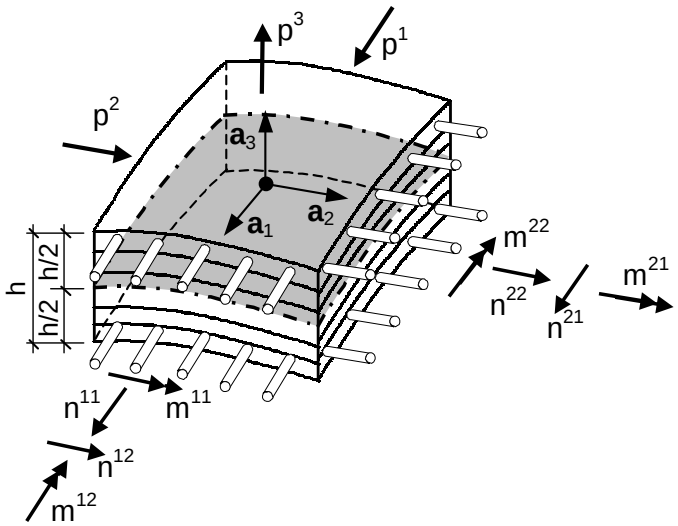

Figure 1. Body forces and stress resultants of a shell.

1 and Equation 2. Symmetric membrane forces which are energy conjugate to the first strain tensor of the middle surface but do not have a physical interpretation (Başar and Krätzig 1985) are computed from Equation 3. Transversal shear forces are not of interest in this formulation since the Kirchhoff-Love restriction applies for this special type of problems considered within this scope.

$$n^{\alpha\beta} = \int_{-h/2}^{h/2} \mu(\theta^3) \cdot [\delta_\lambda^\beta - \theta^3 \cdot b_\lambda^\beta] \cdot \sigma^{\alpha\lambda}(\theta^3)\, d\theta^3 \qquad (1)$$

$$m^{\alpha\beta} = \int_{-h/2}^{h/2} \mu(\theta^3) \cdot \theta^3 \cdot \sigma^{\alpha\beta}(\theta^3)\, d\theta^3 \qquad (2)$$

$$\tilde{n}^{\alpha\beta} = n^{\alpha\beta} + m^{\alpha\lambda} \cdot b_\lambda^\beta \qquad (3)$$

For computation of stress resultants in a reinforced concrete section, the section is divided up into steel layers and concrete layers. Three different types of material laws are used for the modeling of the individual members: a) uniaxial material laws in direction of the reinforcing steel bars, b) a biaxial material law accounting for the non-linear isotropic behaviour of uncracked concrete assuming plane stress in each layer and c) orthotropic material laws for modeling the bond interaction between concrete and steel (tension stiffening) after exceeding the tensile stress.

2.2 *Material law for reinforcing steel*

In Figure 2, the uniaxial elastic-plastic material law for reinforcing steel is depicted. After exceeding the yield limit, hardening starts. For unloading and reloading, the Bauschinger effect is considered. For stress computation, strains are transformed from the original co-ordinate system to the direction of bars. Stresses are obtained in these directions using current strains and plastic history variables. Then, stresses in directions of reinforcing bars are transformed back to the original co-ordinate system and are introduced

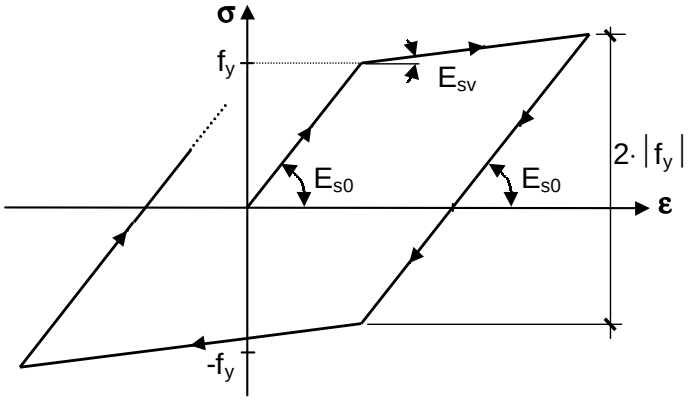

Figure 2. Material law for reinforcing steel.

into the numerical evaluation of Equation 1 and Equation 2.

2.3 *Biaxial material law for undamaged concrete*

For modeling the behaviour of undamaged concrete, a non-linear elastic isotropic material law (Cedolin and Mulas 1984) with numerical realization by Grote (Grote 1992) is applied. This material law contains the failure criterion depicted in Figure 3 and provides an empirical relation for the bulk and shear modulus in dependence of the state of strain based on extensive testing. The two different types of failure are crushing and cracking. For unloading and reloading in the undamaged domain, orthotropic plastic laws in directions of main strain are used (Rahm 2002).

2.4 *Modeling of tension stiffening*

After exceeding the tensile stress of concrete, cracking takes place. In a discrete crack, concrete stresses are zero and the steel stresses exceed a peak value. For the numerical modeling in this contribution, a smeared crack approach is used. Thus, tension stiffening effects are considered by equivalent mean concrete stresses. The relation between mean strains and

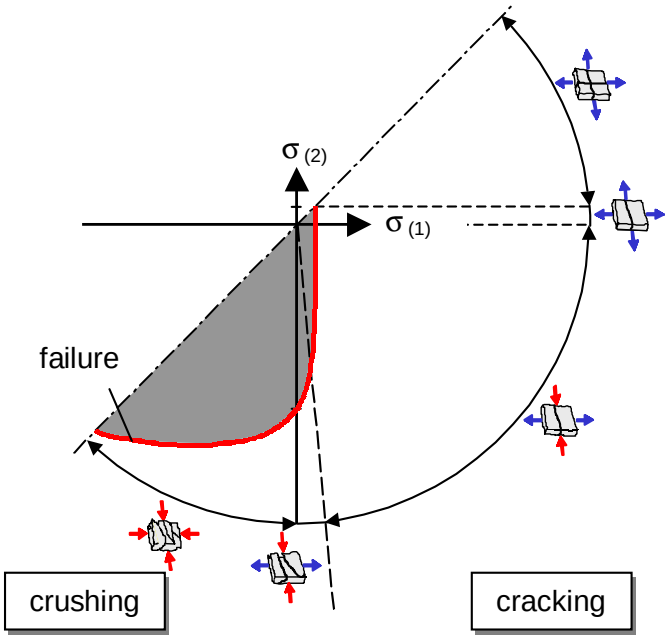

Figure 3. Biaxial behaviour of concrete.

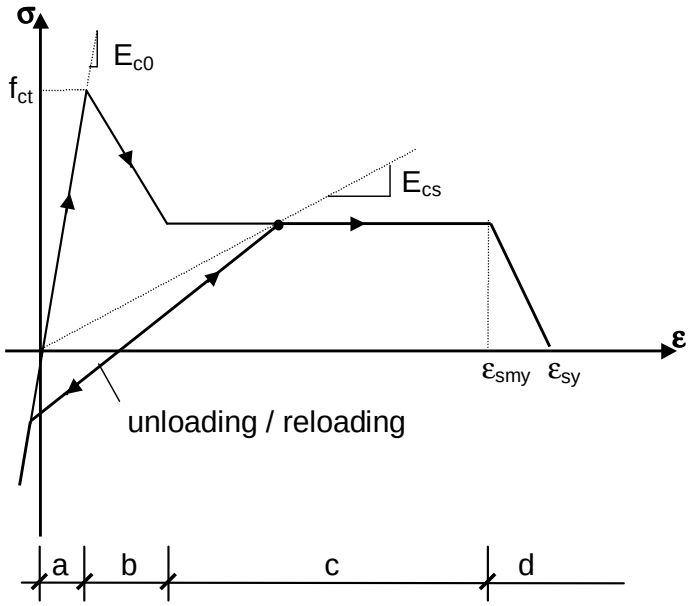

Figure 4. Modeling of tension stiffening with equivalent mean concrete stresses.

mean concrete stresses in cracked regions can be easily derived from the uniaxial material law of a reinforced concrete tension member. The uniaxial tension stiffening law depicted in Figure 4 describes mean concrete stresses. This uniaxial law is applied within an orthotropic formulation in direction of main strain and main stress. Essentially, there are four different regions: a) uncracked concrete before exceeding tensile stress, b) formation of initial cracks, c) completed formation of initial cracks and d) post-yielding. So, equivalent concrete stresses are computed in directions of main strain by evaluating the depicted uniaxial tension stiffening law within an othotropic formulation. Further, damage parameters and history variables are transformed to the current directions of main strain. This accounts for existing cracks during the unloading and reloading process. These processes can be identified as closing and re-opening of cracks. After stress computation in directions of main strain, stresses are updated and transformed to original directions. The same is done with updated history variables. It should be noted that the tension stiffening formulation with equivalent mean concrete stresses is based on the material law of an embedded reinforcing bar. This formulation has advantages for 2D state of stresses and improves convergence behaviour since not all of the concrete layers break down after cracking. However, for uniaxial behaviour of tension truss elements such as supporting truss columns of a shell of revolution, the material law for embedded reinforcement bars is used directly.

3 FINITE ELEMENT MODELING OF SHELLS OF REVOLUTION WITH RING ELEMENTS

3.1 *Geometry and displacement interpolation*

In Figure 5, the geometry of a single ring element as implemented in ROSHE (Wittek et al. 2002) and its degrees of freedom (DOFs) are depicted. By the given relation between height co-ordinate Z and radius $R(Z)$, the geometry of the middle surface is described (Başar and Krätzig 1985). For the actual element, only small strains and small rotations but large deformations of the middle surface are considered. Further, shear deformations are neglected. Assuming a plane of symmetry $x^2 = 0$, the three components of the displacement vector are expressed by a Fourier series with order n_{max} according to Equation 4.

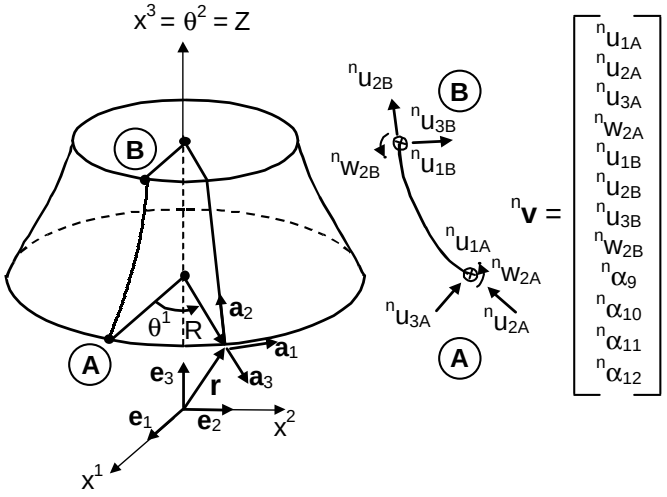

Figure 5. Geometry and degrees of freedom of ring element.

$$\boldsymbol{u}(\theta^1,\theta^2) = \sum_{n=0}^{n_{max}} \begin{bmatrix} {}^n u_1(\theta^2)\cdot sin(n\,\theta^1) \\ {}^n u_2(\theta^2)\cdot cos(n\,\theta^2) \\ {}^n u_3(\theta^2)\cdot cos(n\,\theta^1) \end{bmatrix} \tag{4}$$

For the unknown Fourier coefficients ${}^n u_i$, a finite element approximation is introduced. Cubical polynomials in meridional direction θ^2 are used for each component of the displacement vector. Hence, the proposed ring element must posses 12 DOFs per Fourier term as depicted in Figure 5. DOFs 1–8 relate to the physical nodal displacements and DOFs 9–12 do not have a physical interpretation. They can be either condensed out or assembled into free spaces of the global system vectors and matrices. After that, the unknown displacement field is represented by Equation 5, where ${}^n\boldsymbol{\Phi}$ denotes the array of trial functions for Fourier term n and $\boldsymbol{G}$ represents the transformation matrix for physical DOFs.

$$\boldsymbol{u}(\theta^1,\theta^2) = \sum_{n=0}^{n_{max}} {}^n\boldsymbol{\Phi}\cdot\boldsymbol{G}\cdot{}^n\boldsymbol{v} \tag{5}$$

3.2 *Principle of virtual work for dynamic problems*

The principle of virtual work implies the equilibrium equations in weak formulation. If the total virtual work generated by a virtual displacement vanishes the system is in equilibrium. For dynamic problems, additional inertia and damping forces have to be accounted for.

$$
\begin{aligned}
&\iint_A p^\alpha\,\delta u_\alpha + p^3\,\delta u_3\,dA \\
&+\oint_C n^\alpha\,\delta u_\alpha + n^3\,\delta u_3\,dC \\
&-\iint_A \tilde{n}^{\alpha\beta}\,\delta\alpha_{\alpha\beta} + m^{\alpha\beta}\,\delta\beta_{\alpha\beta}\,dA \\
&-\iint_A \rho\,h\cdot[a^{\alpha\beta}\,\ddot{u}_\alpha\,\delta u_\beta + \ddot{u}_3\,\delta u_3]\,dA \\
&-\iint_A [c_t\,a^{\alpha\beta}\,\dot{u}_\alpha\,\delta u_\beta + c_n\,\dot{u}_3\,\delta u_3]\,dA = 0
\end{aligned}
\tag{6}
$$

In Equation 6, the total virtual work for the shell is given. For the sake of brevity, external moments acting either as traction boundaries or as body forces are neglected here. External damping effects are accounted for in the fifth term of Equation 6 whereas internal damping effects are considered in the resisting forces represented by the third term of Equation 6. For a system with discrete DOFs, Equation 6 yields the well known equations of motion according to Equation 7 which can be also identified as dynamic equilibrium

$$
\boldsymbol{P}_e - \boldsymbol{P}_i - \boldsymbol{P}_m - \boldsymbol{P}_{ce} = \boldsymbol{0} \tag{7}
$$

where $\boldsymbol{P}_e$ = vector of applied forces; $\boldsymbol{P}_i$ = vector of resisting forces; $\boldsymbol{P}_m$ = vector of inertia forces; $\boldsymbol{P}_{ce}$ = vector of external damping forces.

3.3 *Linearization of principle of virtual work*

In general, kinematic and material relations in Equation 6 are non-linear. Thus, Equation 7 cannot be solved directly and therefore has to be linearized. A split-up of all mechanical variables into a current state and increments is required. After introducing the split up of mechanical variables and the FE displacement approximation into the principle of virtual work Equation 6, the element vectors and matrices for the ring element are obtained (Lang 2003).

In general, integration of virtual work expressions for the ring element has to be carried out numerically in both directions using Gauss quadrature in meridional and Simpson integration in circumferential direction. For linear dependency of stresses and strains on displacements, integration in circumferential direction is solved analytically. Due to orthogonality properties of harmonic functions, all off-diagonal matrices for different Fourier terms $n \neq m$ vanish (Lang 2003). The mechanical interpretation shows that the problem is decoupled in Fourier terms; increments in Fourier term m yield force increments in the same Fourier term $n = m$ exclusively. Thus, the linear problem can be set up and solved for every Fourier term independently. However, this nice property is lost when the structure behaves non-linear. The mass and external damping matrix still maintain their super-diagonal structure. Coupling occurs in the tangent stiffness and internal damping matrix with increasing non-linearities. After assembly of element vectors and matrices, the global equation of motion Equation 8 in incremental formulation is obtained. For linear behaviour, Equation 8 simplifies and can be expressed by Equation 9 which is solved directly.

$$
\begin{aligned}
&\boldsymbol{K}_t\cdot\overset{+}{\boldsymbol{V}} + (\boldsymbol{C}_i + \boldsymbol{C}_e)\cdot\overset{+}{\dot{\boldsymbol{V}}} + \boldsymbol{M}\cdot\overset{+}{\ddot{\boldsymbol{V}}} \\
&= \boldsymbol{P}_e - \boldsymbol{P}_i - \boldsymbol{P}_{ce} - \boldsymbol{P}_m
\end{aligned}
\tag{8}
$$

$$
\boldsymbol{K}_e\cdot\boldsymbol{V} + (\boldsymbol{C}_i + \boldsymbol{C}_e)\cdot\dot{\boldsymbol{V}} + \boldsymbol{M}\cdot\ddot{\boldsymbol{V}} = \boldsymbol{P}_e \tag{9}
$$

3.4 *Structural modeling of natural draught cooling towers with ring elements*

One major advantage of modeling shells of revolution with ring elements is the very simple discretisation process. The structure only has to be subdivided in meridional direction into single ring elements by horizontal cuts. The proposed ring element concept which has been derived for a double curved shell ring element in the previous sections can be easily extended to other structural members. For the application study of a hyperbolic natural draught cooling tower which will be examined in section 5, different structural elements are used as can be seen from Figure 6.

The upper ring beam is modeled with a ring beam element. The shell itself is modeled with the proposed double curved ring elements. For the supporting columns, a special discrete column ring element has been developed by the first author as implemented in ROSHE. This macro element consists of single 3D-beams in special equidistant arrangement (A-, V-, X- or I-columns). The nodal DOFs of the single beams are coupled along the upper and lower nodal circle by a Fourier series. By summing up the contributions of all beams, a smeared column ring element consisting of discrete 3D-beams is obtained. For A-, V- and X- columns, non-linearities due to cracking of reinforced concrete can be considered in a simplified way: Therefore, the uniaxial material law of a reinforced tensile member is evaluated in dependence of the axial strain in the centre axis of every single beam. With this law, an equivalent Young's modulus is computed for every beam depending on the state of strain. This accounts for the average stiffness reduction due to cracking caused by tensile normal forces and is a good approach for supporting truss columns where bending moments occur solely at the nodes due to compatibility and are of minor importance compared to axial forces. This is only valid for truss columns in contrast to I-columns. The elastic support of the ground is modeled with a ring spring element. Again, a Fourier series is used for the representation of displacements in circumferential direction. Non-linear behaviour due to uplift can be accounted for by evaluating the circumferential integrals of virtual work expressions numerically.

4 SOLUTION ALGORITHMS FOR EQUATIONS OF MOTION UNDER SEISMIC EXCITATIONS

Ground motion due to earthquake can cause severe damage to structures or in worst case collapse. Special analysis techniques have to be applied to guarantee a safe design against collapse. Basically, ground motions can be regarded as inertia forces acting on a structure in horizontal and vertical direction. In this section, the consideration of inertia forces due to horizontal ground motion in a ring element model of a shell of revolution is shown and the modified equations of motion are set up. Their solution in every time step can be obtained using either linear or non-linear dynamic analysis methods. However, this effort is not justified in general. Simplified analysis methods such as equivalent static acceleration method or response spectrum method are frequently used in structural analysis. But it is pointed out, that for consideration of non-linear dynamic effects analyses in the time domain with given acceleration functions $f(t)$ have to be carried out. In this section, the basic theory of these methods is explained in combination with ring elements. They are further applied to a natural draught cooling tower under horizontal dynamic ground acceleration in section 5 where the results of the different analysis methods and the consequences on the structural design are discussed and compared.

4.1 *Equivalent vector of body forces due to horizontal ground acceleration*

For the description of earthquake acceleration in this contribution, it is assumed that the ground is moving as a rigid body with acceleration $\ddot{v}_{gr} \cdot f(t)$, where $\ddot{v}_{gr}$ = maximum horizontal ground acceleration and $f(t)$ = acceleration function scaled to unit peak value $1.0\ m/s^2$. This yields the vector of physical body forces according to Equation 10 for horizontal ground acceleration, where $\alpha = -arctan(dR(Z)/dZ)$.

$$\boldsymbol{p} = \rho h \cdot f(t) \cdot \begin{bmatrix} \ddot{v}_{gr} \cdot sin(\theta^1) \\ \ddot{v}_{gr} \cdot cos(\theta^1) \cdot sin(\alpha) \\ -\ddot{v}_{gr} \cdot cos(\theta^1) \cdot cos(\alpha) \end{bmatrix} \tag{10}$$

With this relation, the vector of body forces due to acceleration is easily set up which leads to the global load vector after assembly ${}^n\boldsymbol{P}_{gr} = {}^n\boldsymbol{P}_e$. From the dependence of Equation 10 on the circumferential co-ordinate θ^1, it can be readily seen that horizontal earthquake acceleration yields only contributions in Fourier term $n = 1$ (in contrast, vertical ground motion leads to a load vector in Fourier term $n = 0$).

4.2 *Free vibration analysis*

The first step in earthquake analysis must always be the solution of the free vibration problem. This is necessary to get a first important insight into structural dynamic properties described by eigenmodes and eigenfrequencies. Since element mass matrix and linear elastic stiffness matrix are decoupled in Fourier terms (super-diagonal structure), the linear eigenvalue problem of free vibration Equation 11 of a shell of revolution is also independent in Fourier terms:

$$[{}^{nn}\boldsymbol{K}_e - ({}^n_i\omega)^2 \cdot {}^{nn}\boldsymbol{M}] \cdot {}^n_i\boldsymbol{\psi} = \boldsymbol{0} \tag{11}$$

From this, a number of eigenfrequencies and eigenvectors is computed independently for every Fourier term. Due to the discussed orthogonality properties of harmonic functions, solely eigenvectors in Fourier term $n = 1$ participate in the linear dynamic solution and still dominate the non-linear motion significantly among all other Fourier terms.

4.3 *Simplified static analysis methods*

The simplest approach for computation of stresses due to earthquake acceleration is a static analysis with equivalent static acceleration. For the horizontal motion of a shell of revolution, the first eigenperiod ${}^1_1T = 2\pi/{}^1_1\omega$ is obtained from the free vibration problem according to Equation 11. The dynamic amplification factor ${}^1_1\beta$, which relates to the eigenmode with period ${}^1_1T$, is obtained from a given response spectrum as shown in Figure 9. In general, a response spectrum provides the maximum dynamic answer of a single degree of freedom (SDOF) system subjected to ground motion with unit acceleration in dependence of its period T and damping ratio ξ. So, with this dynamic amplification factor, a static load vector according to Equation 10 is set up where the time scaling factor $f(t)$ is substituted by the response factor ${}^1_1\beta$.

A simple static analysis is carried out with this equivalent load vector to obtain stresses due to earthquake. It should be noted that the equivalent static acceleration depends only on the first period of Fourier term $n = 1$, higher modes are not considered. Further, the distribution of these equivalent acceleration does not depend on the shape of the eigenmode. This method can be advantageously applied for cooling towers if the eigenmode of the shell describes a rigid body motion of the shell on the supporting columns.

A more advanced and more appropriate method for computation of stresses due to earthquake can be found in response spectrum method. Basically, this method derives from the modal analysis method shown in the next section. After decoupling the system of linear equations of motion, the problem is expressed by a number of independent equations each representing a SDOF oscillator according to Equation 12 where i = current participating mode; q = generalized co-ordinate of motion.

$${}^n_i\ddot{q} + 2\,{}^n_i\xi\,{}^n_i\omega \cdot {}^n_i\dot{q} + ({}^n_i\omega)^2 \cdot {}^n_i q = \frac{{}^n_i\boldsymbol{\psi}^T \cdot {}^n\boldsymbol{P}_{gr}}{{}^n_i m} \tag{12}$$

For every SDOF oscillator, the solution for the maximum acceleration is obtained from the response spectrum according to Equation 13.

$$max\ {}_i^n\ddot{q} = {}_i^n\beta \cdot \frac{{}_i^n\boldsymbol{\psi}^T \cdot {}^n\boldsymbol{P}_{gr}}{{}_i^n m} \tag{13}$$

For horizontal ground motion, solely eigenvectors $n = 1$ contribute since load vector ${}^n\boldsymbol{P}_{gr}$ is zero for $n \neq 1$. This leads to an equivalent static load vector for every eigenvector ${}_i^n\boldsymbol{\psi}$ according to Equation 14.

$${}_i^n\tilde{\boldsymbol{P}}_{gr} = {}^{nn}\boldsymbol{M} \cdot {}_i^n\boldsymbol{\psi} \cdot {}_i^n\beta \cdot \frac{{}_i^n\boldsymbol{\psi}^T \cdot {}^n\boldsymbol{P}_{gr}}{{}_i^n m} \tag{14}$$

A static analysis is carried out for every eigenvector i of Fourier term $n = 1$. The stresses obtained for each eigenvector are combined by SRSS or CQC rule, depending on the correlation of frequencies (Chopra 2001).

4.4 *Solution algorithms for transient linear dynamic problems*

In this section, methods for solving the system of linear equations of motion Equation 9 for a time – acceleration relation of a given earthquake are discussed. Basically, it has to be distinguished between direct integration and modal analysis. In direct integration, time derivatives are substituted by difference quotients of displacements. Thus, Equation 9 is transformed into an algebraic equation and solved directly. Special restrictions on the selection of the time step size have to be satisfied in order to ensure integration stability and accuracy.

A different method can be found in modal analysis which is a classical linear method since the problem is split up into mode contributions. These are solved independently and assembled again. Here, the physical DOFs are substituted by eigenvectors times generalized co-ordinates according to Equation 15. By transformation of Equation 9, equivalent quantities of a SDOF system are established for every contributing mode as defined in Equations 16 – 20.

$$\begin{aligned} {}^n\boldsymbol{V} &= \sum_i {}_i^n\boldsymbol{\psi} \cdot {}_i^n q \qquad {}^n\dot{\boldsymbol{V}} = \sum_i {}_i^n\boldsymbol{\psi} \cdot {}_i^n\dot{q} \\ {}^n\ddot{\boldsymbol{V}} &= \sum_i {}_i^n\boldsymbol{\psi} \cdot {}_i^n\ddot{q} \end{aligned} \tag{15}$$

$${}_i^n k = {}_i^n\boldsymbol{\psi}^T \cdot {}^{nn}\boldsymbol{K}_e \cdot {}_i^n\boldsymbol{\psi} \qquad \text{modal stiffness} \tag{16}$$

$${}_i^n m = {}_i^n\boldsymbol{\psi}^T \cdot {}^{nn}\boldsymbol{M} \cdot {}_i^n\boldsymbol{\psi} \qquad \text{modal mass} \tag{17}$$

$${}_i^n\omega = \sqrt{\frac{{}_i^n k}{{}_i^n m}} \qquad \text{circ. frequency} \tag{18}$$

$${}_i^n c = 2 \cdot {}_i^n\xi \cdot {}_i^n\omega \cdot {}_i^n m \qquad \text{modal damping} \tag{19}$$

$${}_i^n p = {}_i^n\boldsymbol{\psi}^T \cdot {}^n\boldsymbol{P}_e \qquad \text{modal force} \tag{20}$$

Advantages of modal analysis can be found in a) the analytical integration of equivalent SDOF oscillators, b) the reduction of the total number of DOFs to a small number of participating modes, c) the consideration of damping by critical damping ratios ξ so that no damping matrix has to be recalculated from Rayleigh damping parameters or critical damping ratios and d) the physical insight into the dynamic behaviour expressed in participating modes.

4.5 *Solution algorithms for transient non-linear dynamic problems*

In non-linear dynamics, the system of equations of motion is expressed by Equation 7. However, it cannot be solved directly due to non-linear dependence of system properties on the current state. Incremental iterative solution strategies have to be applied to the linearized system of equations of motion Equation 8. For non-linear structural behaviour, direct integration schemes work almost the same as for linear behaviour. The difference consists in the formulation in displacement, velocity and acceleration increments. From a given state of equilibrium of the last time step, the time is increased which results in a change of effective load due to change in the external forces and due to the motion. The first solution of the new variables of motion for a new time step is calculated in the increment step (predictor step). After that, equilibrium is checked with the updated state. However, it is most likely not to be satisfied due to the linearization error. Iteration steps (or corrector steps) are applied until the convergence criterion is satisfied (out of balance forces must vanish). Actually, in every increment or corrector step the problem is reduced to the problem of a linear static analysis using an effective stiffness which consists of a combination of $\boldsymbol{K}_t$, $\boldsymbol{C}$, $\boldsymbol{M}$ and an effective load vector. The adaptation of Newmark's method to this incremental iterative formulation as an example for all implicit direct integration schemes is shown and discussed in (Lang 2003). It should be noted that for non-linear structural response the off-diagonal terms ($n \neq m$) are fully occupied. The problem cannot be decoupled in Fourier terms. However, these off-diagonal terms are of minor importance in the effective stiffness matrix due to contributions of the super-diagonal mass matrix and Rayleigh damping matrix and can be neglected in the solution process (modified Newton type algorithm). Hence, the use of direct integration schemes in combination with ring elements becomes very effective. The importance of mass contribution even increases quadratically with smaller time steps.

For non-linear problems, the application of modal analysis is not known very well since the principle of superposition is no longer valid. However, with a few modifications it can be adapted to non-linear problems as recently shown for earthquake analysis of steel frames (Khudada and Geschwindner 1997) and for impact on concrete cubes (Bucher 2000). The non-linear formulation of modal analysis has been further successfully applied to the proposed non-linear formulation of ring elements and validated by the first author (Lang 2003). Due to the dependence on the current state, the equations of motion have to be solved iteratively anyway and cannot be decoupled for the whole time domain. Nevertheless, a modal superposition in a linearized increment or iteration step is still valid.

Again, modal quantities can be identified. But now, the problem is solved independently in a linearized (predictor or corrector) step for every contributing mode where contributions arising from off-diagonal terms $(i \neq j)$ are neglected due to minor importance. It should be noted, that modal stiffness and modal out of balance forces have to be updated after every linearized step. Advantages of the non-linear formulation against direct integration are a) the less severe requirements in the time step size resulting in less computational costs, b) the reduction of DOFs for the representation of the motion, c) the consideration of every participating mode with the same accuracy and d) the better insight into structural behaviour due to modal representation. But it should be also noted that the number of required modes for the representation of motion and stresses increases dramatically compared to linear problems. Further details are not discussed here and can be found in (Bucher 2000) and (Khudada and Geschwindner 1997), for the special case of ring elements in (Lang 2003).

5 APPLICATION STUDY FOR NATURAL DRAUGHT COOLING TOWER

5.1 *Geometry, loading and safety concept*

The proposed ring element concept in combination with the analysis methods for dynamic problems are applied to a natural draught cooling tower with a total height of approximately $180\ m$ in order to clarify its structural behaviour under horizontal earthquake acceleration. The system is depicted in Figure 6, the corresponding numerical model consists of a ring beam element at the upper edge, 43 double curved shell ring elements, a discrete V-column macro element with 46 column pairs, a second ring beam element for modeling the ring foundation and a vertical translation ring spring element accounting for the vertical soil stiffness.

The reinforcement amounts for the non-linear earthquake analyses have been computed by linear static analysis according to the static load combinations defined in BTR 97 (VGB 1997). Maximum total reinforcement amounts in ring direction of $a_{s1} =$

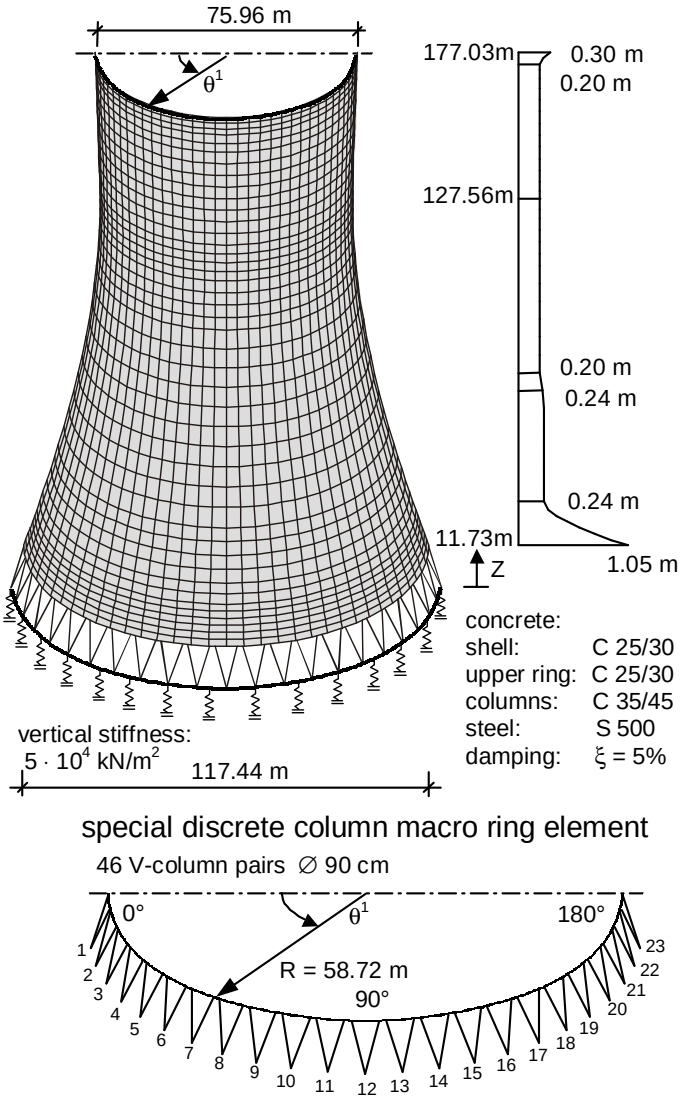

Figure 6. Geometry of natural draught cooling tower and FE-model.

$16.0\ cm^2/m$ and in meridional direction of $a_{s2} = 19.7\ cm^2/m$ are provided. A total horizontal ground acceleration = $3.50\ m/s^2$ which already contains the importance factor is applied to the structure. On the MSK intensity scale from I – XII, this acceleration can be found approximately between zone IX and X. Zones X – XII are so strong that a design against these is not feasible in most cases from the technical and economical point of view (definition of zone XII: destruction of all structures).

For dynamic transient analyses with direct integration or modal analysis, different unit acceleration functions $f(t)$ are used which are depicted in Figure 7. These are taken from the Kern County earthquake (21.07.1952, Taft Lincoln School), the Imperial Valley earthquake (19.05.1949, El Centro) and the San Fernando earthquake (09.02.1971, Pacoima Dam). For dynamic analysis, the maximum acceleration $\ddot{v}_{gr} = 3.50\ m/s^2$ is scaled by $f(t)$ for every time step.

The European safety concept of Eurocode 1 and Eurocode 8 requires a section design according to Equation 21. No additional live load is acting in combination with earthquake. For cooling towers as struc-

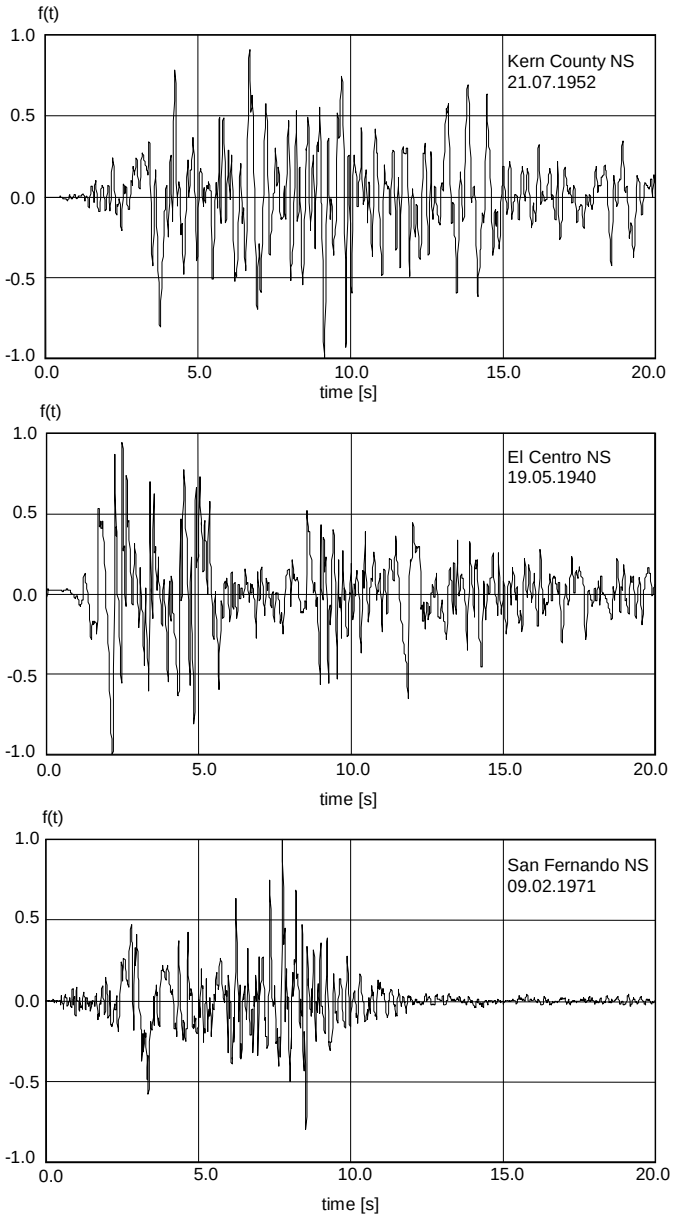

Figure 7. Horizontal ground acceleration of selected earthquakes.

tures of special importance, an importance factor of $\gamma_I = 1.4$ at the upper bound is justified. An importance factor $\gamma_I = 1.0$ relates to the intensity of an earthquake with return period of 475 years.

$$S_d(g + \gamma_I \cdot e) \leq R_d(\alpha \cdot f_{ck}/\gamma_c,\ f_{yk}/\gamma_s) \tag{21}$$

The section resistance R_d is calculated according to different design standards depending on the material – in the special case of reinforced concrete according to Eurocode 2. The partial material safety factors for computation of section resistance can be reduced compared to regular design situations ($\gamma_c = 1.3$, $\gamma_s = 1.0$).

5.2 *Free vibration behaviour*

For dynamic analysis of a shell of revolution subjected to horizontal ground motion, the eigenmodes and eigenperiods of Fourier term $n = 1$ are of special interest. The linear dynamic solution is decomposed solely by these eigenvectors. In non-linear dynamic analysis they still provide the most important contribution to the total solution. Thus, the first step in earthquake analysis is always to solve Equation 11 for Fourier term $n = 1$. Eigenmodes $i = 1 - 3$ in Fourier term $n = 1$ are depicted in Figure 8 for the geometry of the presented natural draught cooling tower. The first eigenmode with period $T = 0.731\ s$ essentially describes a rigid body rocking on the vertical elastic support of the ground. In contrast, the second eigenmode with period $T = 0.401\ s$ is essentially a rigid body motion from side to side on the elastic column support. This motion is responsible for very high tensile and compressive forces in the supporting trusses close to circumferential angle $\theta^1 = 90°$. The period of the third eigenmode $T = 0.181\ s$ is much more smaller than the first and second period since the shell does no longer behave as an idealized rigid body. This becomes also obvious from the shape of the third eigenmode in Figure 8. Here, high axial strains in meridional direction occur especially in the region around meridional height $Z = 140\ m$. Further, the computed periods are shown in the response spectrum diagram Figure 9. The corresponding eigenmodes are used for the determination of linear structural response in this study in the next section.

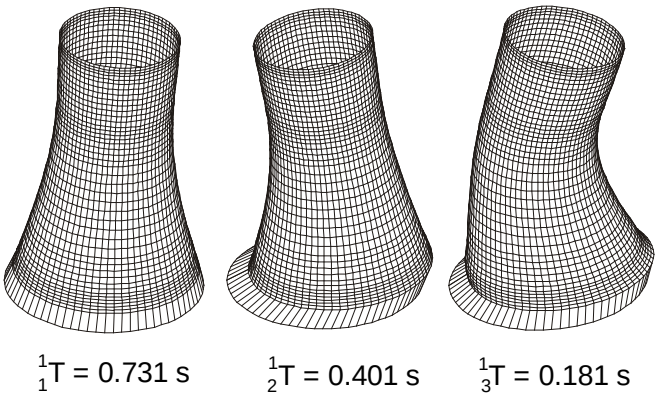

Figure 8. Eigenvectors of cooling tower for Fourier term n = 1.

5.3 *Linear results for earthquake load combination*

The linear structural response is computed with different methods: These are on the one hand side simplified analysis methods using equivalent static acceleration or response spectrum method and on the other hand dynamic analyses for different unit acceleration functions $f(t)$ as depicted in Figure 7. The equivalent static acceleration is obtained from the EC 8-A response spectrum in Figure 9. For the first period $T = 0.731\ s$, a dynamic amplification factor $\beta = 1.67$ can be found which is the only eigenmode to be used in equivalent static acceleration method. This yields an equivalent static acceleration $\beta \cdot \ddot{v}_{gr} = 1.67 \cdot 3.5\ m/s^2 = 5.86\ m/s^2$. It should be noted that for the first period the response spectrum of the El Centro earthquake matches the EC 8-A spectrum very good. The San Fernando earthquake, however, yields a dynamic amplification $\beta << 1.67$ for the first period

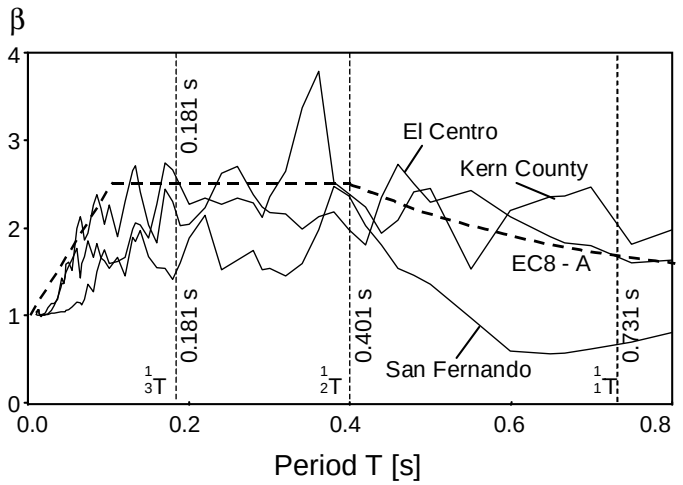

Figure 9. Response spectra of selected earthquakes.

and the Kern County earthquake results in a higher amplification than El Centro and EC 8-A spectrum $\beta > 1.67$. This fact can be found in the results of transient analysis again.

The most important linear results are summarized in Table 1 for different analysis methods for $g + 3.50\ m/s^2$. They are further compared with results from linear static analysis for wind load combination $g + 1.75w$ respectively $1.75(g + w)$ according to BTR 97. From Table 1, it can be seen that the static analysis with equivalent acceleration forces $\beta \cdot \ddot{v}_{gr} = 5.86\ m/s^2$ yields good results solely for the maximum soil pressure max P_{ground} and for the minimum and maximum column forces min P_{column} and max P_{column}. These can be used for the design of column reinforcement amounts. However, the results for the shell expressed by the cracking load factor λ and maximum meridional force max n^{22} do not agree at all and therefore can not be used for the design. As a significant fact, it is emphasized that the equivalent static acceleration method yields only good results for the foundation and supporting columns.

Response spectrum method yields essentially the same results as linear dynamic time domain analysis for given function $f(t)$ of the El Centro earthquake. This becomes also clear from Figure 9 since the response spectrum according to Eurocode 8-A matches the El Centro spectrum best for the important eigenperiods. Kern County earthquake generates the maximum meridional force $n^{22} = 1014\ kN/m$.

Table 1. Linear results for selected earthquakes in comparison with simplified methods.

	max n^{22} [kN/m]	max P_{ground} [kN/m²]	uplift g+λ·e	first crack g+λ·e	min P_{column} [kN]	max P_{column} [kN]
static acceleration	331	513	g+0.98·e	g+1.30·e	-13057	+ 5864
resp. spectr. method	595	533	g+0.91·e	g+0.94·e	-12152	+ 4959
El Centro	578	514	g+0.98·e	g+0.95·e	-13048	+ 5829
Kern County	1014	630	g+0.68·e	g+0.69·e	-12759	+ 5539
San Fernando	99	356	g+2.55·e	g+1.74·e	-10859	+ 3642
BTR 97 [20]	808 [1)]	586 [2)]	g+1.82·w [3)]	g+1.36·w [3)]	-10746 [2)]	+ 1054 [1)]

[1)] g + 1.75·w [2)] 1.75 · (g + w) [3)] g + λ·w

San Fernando earthquake, however, results in a maximum meridional force of $n^{22} = 99\ kN/m$ for the same acceleration $3.50\ m/s^2$. This behaviour can be also found in Figure 9 since the amplification for the first eigenmode subjected to San Fernando earthquake is very small compared to the El Centro and Kern County earthquake.

In Figure 10, the required reinforcement quantities in meridional direction a_{s2} (total quantity for the whole section) and maximum meridional forces n^{22} are plotted over the height of the shell. From this, it can be readily seen that for the design of the shell the earthquake load combination does not become relevant in general compared to static load combinations of BTR 97. Only the very strong Kern County earthquake yields higher meridional forces n^{22} and thus higher required meridional reinforcement quantities a_{s2} than static wind load combinations according to BTR 97 in the lower part of the shell $Z < 80\ m$ (colored with grey).

The following non-linear dynamic analyses in the time domain will only be carried out with El Centro and Kern County earthquake. Uplift of the foundation from ground takes place for $g + 3.43\ m/s^2$ $(\lambda = 0.98)$ for El Centro earthquake and $g + 2.38\ m/s^2$ $(\lambda = 0.68)$ for Kern County earthquake, so that significant non-linear effects will be expected in the shell due to cracking and uplift in the foundation for these two earthquakes. For the San Fernando earthquake, cracking of the shell and uplift do not occur under load combination $g + 3.50\ m/s^2$. However, cracking of columns will happen for all examined earthquakes since the cracking axial force $N = 2300\ kN$ is exceeded by far. However, this is not the case for static load combination $g + 1.75w$. These non-linear effects will be clarified in the following sections with non-linear dynamic analyses in the time domain for El Centro and Kern County earthquake.

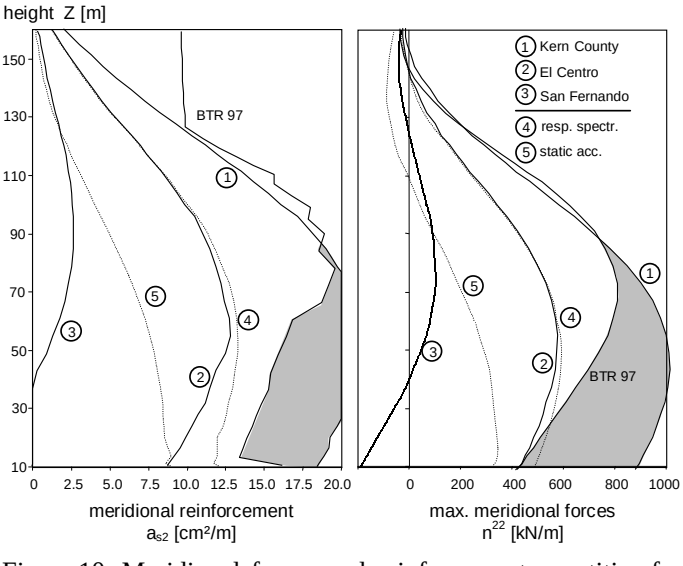

Figure 10. Meridional forces and reinforcement quantities for linear behaviour.

5.4 *Non-linear dynamic results (uplift)*

In a first approximation step, uplift of the foundation from the ground is considered as the only non-linearity for the El Centro and Kern County earthquake so that tensile forces between the ring foundation and supporting ground cannot be transferred. Significant results (maximum meridional forces n^{22} and corresponding required reinforcement amount a_{s2}) for the shell are depicted in Figure 11.

It can be found that the maximum tensile meridional force caused by the Kern County earthquake is decreased from $1014\,kN/m$ to $780\,kN/m$ (approx. 23%). This yields a reduction of maximum required meridional reinforcement $a_{s2} = 17.0\,cm^2/m$ (compared to linear result $22.2\,cm^2/m$). However, for the El Centro earthquake no significant changes in results for the shell can be found since the system is just about to uplift (uplift factor $\lambda = 0.95$). According to Figure 11, the required reinforcement amounts and meridional forces for earthquake load combination are lower than those due to static load combinations (linear statics, requirements by BTR 97) so that for the design of the shell the earthquake load combination does not play an important role. It should be noted, that consideration of uplift as the only non-linearity has the significant advantage that the results are not depending on reinforcement amounts and can be directly used for the design.

Further, column tensile forces are reduced in the uplifting regions around $\theta^1 = 0°$ and $\theta^1 = 180°$. However, the maximum tensile column forces cannot be found in these regions. They occur between $\theta^1 = 60°$ and $\theta^1 = 120°$ since high horizontal forces have to be transferred to the ground by the columns in these regions. The aspect of cracking of columns and shell and the consequences on forces and structural design are discussed more extensively in the following section.

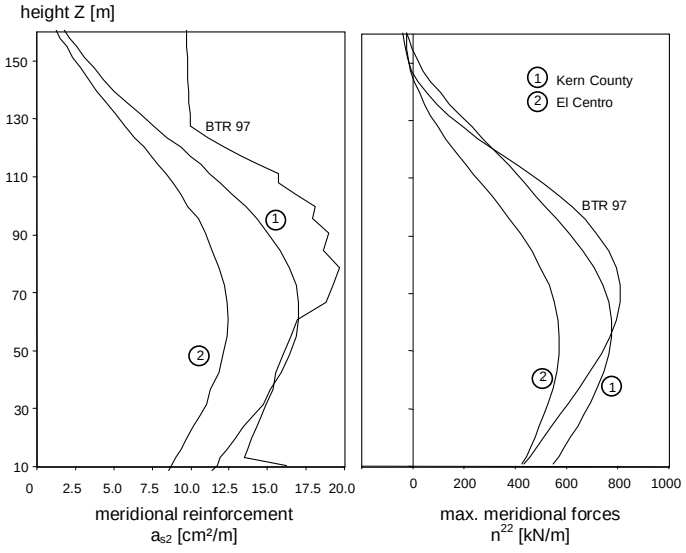

Figure 11. Meridional forces and reinforcement quantities for non-linear behaviour (uplift).

5.5 *Non-linear dynamic results (uplift, non-linear behaviour of shell and columns)*

In a second step, the non-linear behaviour of reinforced concrete is additionally taken into consideration for the numerical calculations. For the shell, the realistic material laws are accounted for within the presented numerical layer model for the cross-section in the ring element formulation. Here, significant changes are only expected for the Kern County earthquake. Further, the supporting columns are modeled with a macro column ring element where an idealized material law for uniaxial truss elements is used to account for stiffness reduction due to cracking.

The results for the shell are depicted in Figure 12. Here, it can be seen that for the El Centro earthquake no significant changes in meridional stresses and in required reinforcement amounts occur compared to Figure 11, because cracking is just about to happen for the design acceleration $3.50\,m/s^2$. For the Kern County earthquake, the meridional forces n^{22} and required reinforcement amounts are reduced again compared to Figure 10 and Figure 11. Thus, a total reduction in meridional forces of 37% (from linear solution $1014\,kN/m$ to non-linear solution $634\,kN/m$ including uplift and cracking of concrete) can be observed. The shell itself is able to resist the earthquake load combination $g + 3.50\,m/s^2$ if it has been properly designed with linear static analysis against static load combinations as required in BTR 97.

As discussed earlier, the tensile column forces are approximately five times higher than those from wind load combination $g + 1.75w$. The cracking force $N = 2300\,kN$ is exceeded by far. This effect has major importance compared to other non-linear effects. Thus, the cracking of columns due to axial tensile force is also accounted for in the non-linear calculations which are based on a column reinforcement amount $A_{s,col} = 162\,cm^2$ from the linear earthquake design.

For the Kern County earthquake, the results for

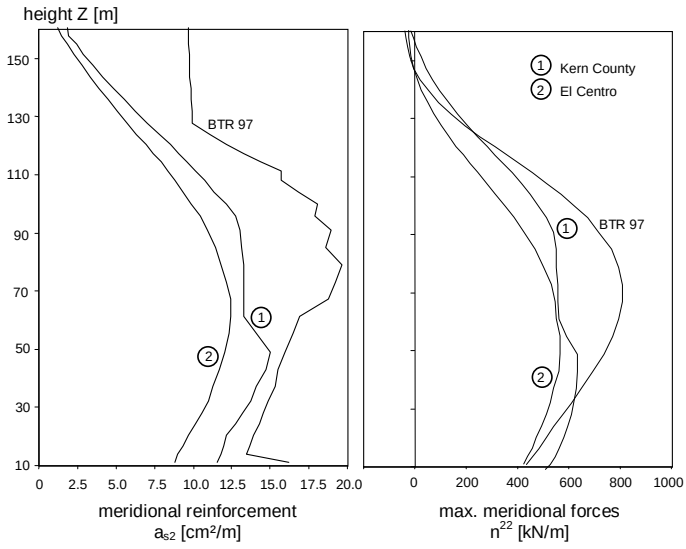

Figure 12. Meridional forces and reinforcement quantities for non-linear behaviour (uplift and cracking).

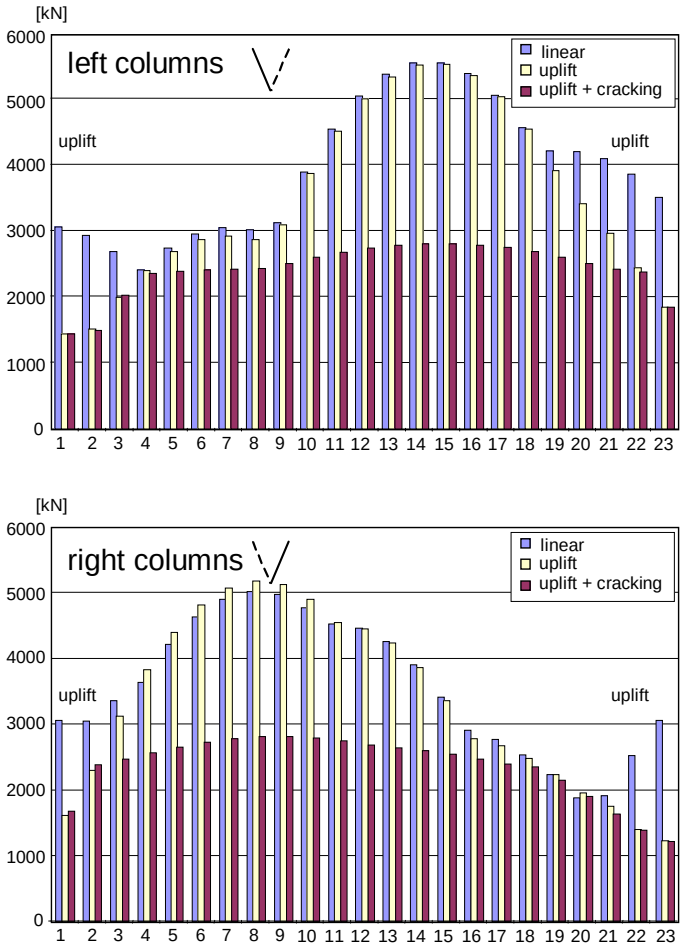

Figure 13. Distribution of maximum column tensile forces for Kern County earthquake.

maximum tensile forces can be found in Figure 13. Here, the linear results, the results with consideration of uplift and the results with consideration of uplift, cracking of shell and cracking of columns are depicted for all columns from $\theta^1 = 0°$ to $\theta^1 = 180°$. The maximum values can be found at column pair 9 ($\theta^1 \approx 66°$) or 15 ($\theta^1 \approx 114°$). The maximum column tensile force decreases from $5539\,kN$ to $2800\,kN$ by approximately 50%. This value can be confirmed for other earthquakes (Lang 2003). It can be clearly seen that due to uplift the maximum column forces do not change significantly. Only column forces around $\theta^1 = 0°$ and $\theta^1 = 180°$ decrease in the uplifting regions which are not relevant for the structural design. The relevant column tensile forces in the region from $\theta^1 = 60°$ to $\theta^1 = 120°$ decrease due to cracking (cracking force $2300\,kN$) and the loss of stiffness. For the linear structural design of columns, the column with maximum tensile force requires maximum reinforcement. After cracking of columns, it should be noted that the column with maximum tensile force and the column with maximum required reinforcement do not coincide any longer since column bending moments gain importance after cracking (Lang 2003).

It can be readily seen that column tensile forces are the most significant result for the structural design under horizontal earthquake excitations. Compressive column forces, however, are of minor interest since they are of same order as under static wind load combination. The given earthquake combination $g + f(t) \cdot e$ requires a reinforcement amount of $162\,cm^2$ per column (linear design). For comparison purpose, only $56\,cm^2$ reinforcement (minimum reinforcement) are required for the columns to resist wind combination $g + 1.75w$ respectively $1.75(g + w)$.

According to the results gained from this application study, a behaviour factor q can be computed for the reduction of column forces. The behaviour factor q as defined in Eurocode 8 accounts for the non-linear dissipation mechanisms which have been neglected in linear dynamic analysis. Thus, linear stresses due to earthquake acceleration can be reduced for the design by factor q according to Equation 22.

$$S_{d,linear}(g + \gamma_I \cdot e/q) \stackrel{!}{=} S_{d,non-linear}(g + \gamma_I \cdot e) \quad (22)$$

With dead load solution for column forces $N_g = -3500\,kN$, a behaviour factor of $q = 1.5$ can be computed for the given cooling tower geometry subjected to Kern County earthquake with load combination $g + 3.5\,m/s^2$ which has been validated for other earthquakes with same intensity (Lang 2003). It should be noted that this reduction factor only accounts for non-linear effects due to uplift, cracking of shell and cracking of supporting truss columns and can be regarded as a lower bound. Other dissipative effects – especially locally dissipative behaviour in the column joints or the damage of bond of reinforcing bars have not been accounted for in this study. For the final design of column reinforcement, bending moments also have to be considered. Thus, the required column reinforcement is not reduced by 50% corresponding to the reduction of axial forces, but by approximately 44%.

6 SUMMARY AND CONCLUSIONS

In this paper, a non-linear formulation of ring elements has been presented for non-linear dynamic earthquake analysis of shells of revolution. The basic aspects of the derivation of element matrices have been discussed and ideas for adaptation of this ring element concept to other structural members (e.g. ring spring element, macro column element, ring beam element) have been given. Further, methods for solving the equations of motion of a shell of revolution under horizontal earthquake acceleration have been summarized. These are equivalent static acceleration method, response spectrum method and linear or non-linear dynamic analysis in the time domain for given acceleration functions by direct integration schemes or modal analysis. With these methods, the structural behaviour of a natural draught cooling tower with height of approximately $180\,m$ has been clarified. The most important results of this study are summarized in the following: Stresses in the shell due to earthquake are of same order as stresses due to wind load combination according to BTR 97. The dynamic response is

significantly depending on the frequency spectrum of the ground motion which can be obtained from the response spectrum.

For the design of the shell, the static load combinations given in BTR 97 become relevant in general. For a very strong earthquake (in this case Kern County acceleration), it is recommended to carry out the non-linear analysis solely with consideration of uplift. This yields sufficient stress reduction in the shell and the results do not depend on the provided reinforcement amounts. The additional consideration of cracking of the shell generates further stress reduction.

However, the critical regions of the system are the columns since high horizontal forces must be transferred to the ground. The maximum and minimum linear stresses in the columns can be calculated by equivalent static acceleration method with sufficient accuracy. The maximum compressive forces are of same order as under wind load combination $1.75(g + w)$, but the maximum tensile forces exceed those under wind load combination $g + 1.75w$ by factor 5 which results in extensive cracking of the column sections. By considering cracking of columns within non-linear dynamic analyses in the time domain, the column forces for earthquake combination $g + 3.50\, m/s^2$ are reduced by approximately 50% for different earthquakes. This results in a behaviour factor $q > 1.50$ which can be regarded as a lower bound for the column tensile forces. The consideration of non-linear effects for the truss columns have been accounted for in a simplified way with this method. Local dissipative effects have not been considered in this model.

It should be noted that all shown results and comparisons relate to the presented geometry as a special demonstration object and therefore should not be generalized. However, the presented finite element concept and numerical algorithms for linear and nonlinear dynamic analyses provide a very powerful tool for complex simulation and practical earthquake resistant design for shells of revolution.

REFERENCES

Başar, Y. and W. B. Krätzig 1985. *Mechanik der Flächentragwerke*. Braunschweig: Verlag Vieweg & Sohn.

Bucher, C. 2000. Anwendung der Modalanalyse auf Probleme der nichtlinearen Dynamik. In C. Bucher (ed.), *6. Institutskolloquium des Instituts für Strukturmechanik der Bauhaus-Universität Weimar (Bericht 1/00)*, Weimar, pp. 79–84.

Cedolin, L. and M. G. Mulas 1984. Biaxial Stress-Strain Relation for Concrete. *Journal of Engineering Mechanics 110*(2): 187–206.

Chopra, A. K. 2001. *Dynamics of Structures, Theory and Applications to Earthquake Engineering* (2. ed.). Upper Saddle River (New Jersey): Prentice Hall.

Eckstein, U., W. B. Krätzig, and U. Wittek 1980. Finite-Element-Berechnungen zur Grenztragfähigkeit der Rotationsschalen. IKIB-TWM 80-4, Ruhr-Universität Bochum.

Grote, K. 1992. Theorie und Anwendung geometrisch und physikalisch nichtlinearer Algorithmen auf Flächentragwerke aus Stahlbeton. Bericht 1992/1, Fachgebiet Baustatik Universität Kaiserslautern.

Khudada, A. E. and L. F. Geschwindner 1997. Nonlinear Dynamic Analysis of Steel Frames by Modal Superposition. *Journal of Structural Engineering 123*(11): 1519–1527.

Lang, C. 2003. Beitrag zur Theorie, Numerik und Anwendung nichtlinearer Algorithmen zur statischen und dynamischen Analyse von Stahlbetonrotationsschalen. Bericht 2003/1, Fachgebiet Baustatik Universität Kaiserslautern.

Leimbach, K. R. 1973. Eine Methode zur Berechnung der Schwingungscharakteristika ringversteifter Rotationsschalen. Dissertation, Ruhr-Universität Bochum.

Popov, E. P., J. Penzien, and Z.-A. Lu 1964. Finite Element Solution for Axissymmetrical Shells. *Journal of the Engineering Mechanics Division 90*(5): 119–145.

Rahm, H. 2002. Modellierung und Berechnung von Alterungseffekten bei Stahlbetonflächentragwerken. Bericht 2002/1, Fachgebiet Baustatik Universität Kaiserslautern.

VGB 1997. VGB-Fachausschuss Bautechnik bei Kühltürmen: Bautechnische Richtlinien. VGB-Verlag, Essen.

Wittek, U., R. Meiswinkel, and C. Lang 2002. Handbücher zu dem FE-Programm ROSHE. Interner arbeitsbericht, Fachgebiet Baustatik Universität Kaiserslautern.

Wunderlich, W. and H. J. Rensch 1981. A Semi-Analytical Finite Element Process for Nonlinear Elastoplastic Analysis of Arbitrarily Loaded Shells of Revolution. In J. Stalpaert (ed.), *Transactions of the 6th International Conference on Structural Mechanics in Reactor Technology*, Paris.